NASA TECHNICAL NOTE

NASA TN D-3654

NASA TN D-3654

AN ANALOG STUDY OF THE PASSIVE THERMAL BEHAVIOR OF AN ORBITING SPACE STATION

by Lenwood G. Clark and John W. Wilson

Langley Research Center
Langley Station, Hampton, Va.

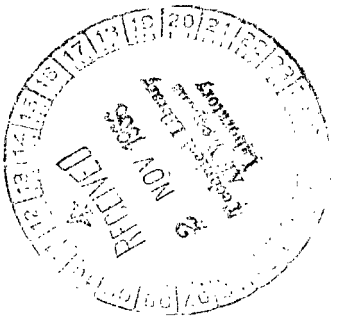

NATIONAL AERONAUTICS AND SPACE ADMINISTRATION • WASHINGTON, D. C. • OCTOBER 1966

NASA TN D-3654

AN ANALOG STUDY OF THE PASSIVE THERMAL BEHAVIOR OF AN ORBITING SPACE STATION

By Lenwood G. Clark and John W. Wilson

Langley Research Center
Langley Station, Hampton, Va.

NATIONAL AERONAUTICS AND SPACE ADMINISTRATION

For sale by the Clearinghouse for Federal Scientific and Technical Information
Springfield, Virginia 22151 – Price $2.00

AN ANALOG STUDY OF THE PASSIVE THERMAL BEHAVIOR OF AN ORBITING SPACE STATION

By Lenwood G. Clark and John W. Wilson
Langley Research Center

SUMMARY

A relatively simple procedure for determining the passive thermal-control capability of an example space station is presented. Approximate Fourier heat equations governing the heat flow through the assumed multilayer wall structure of the spacecraft were solved by means of a general-purpose analog computer. The thermal behavior of the spacecraft was determined for a number of surface-coating distributions. Of these, the surface-coating distribution which provided the least circumferential temperature gradient was selected and the passive thermal-control capability of the spacecraft was determined for a range of orbit conditions. Comparison of steady-state and transient solutions showed that the steady-state solution underestimated the passive heat-transfer capability of the spacecraft.

The analog computer, with its usual ease of changing parameters and rapidity of solution, proved to be relatively economical. An analytical solution of linearized equations was in good agreement with the corresponding analog solution.

INTRODUCTION

For the past decade, increasing amounts of the literature have indicated the importance of temperature in the design of a spacecraft. The thermal design of any spacecraft is subject to the stringent temperature limitations imposed by each of its onboard components, whether they be man or machine. The degree to which the thermal design is integrated into the structural design depends not only upon the required component temperature regimes, but also upon the method of thermal control used.

From the reliability standpoint, passive thermal control achieved at the time of construction by the application of proper optical coatings, careful selection of the spacecraft geometry, and judicious selection of construction materials (ref. 1) would be desirable. However, in many instances it must be supplemented by active thermal-control devices to achieve the required temperature levels.

The purpose of this report is to present a relatively simple method by which estimates can be made of the passive thermal-control capability for providing an optimum living and working thermal environment for the crew members of a manned spacecraft. As an example, the report considers the thermal control during the long-term orbital phase (1 to 5 years) of a large (150-foot-diameter (45.7-m)) hexagonal space station concept shown in figure 1. Knowledge of the thermal mission requirements of the vehicle will permit estimates of the degree of active thermal control which will be required to maintain desired temperatures. On this basis, the vehicle can either be redesigned, if it appears necessary, or the present design can be analyzed more rigorously to define its thermal-control requirements more precisely.

SYMBOLS

The units for the physical quantities used in this paper are given both in U.S. Customary Units and in the International System (SI). Factors relating these two systems of units are given in reference 2.

A	semimajor axis of orbit ellipse, nautical miles
a	earth albedo, dimensionless
C	thermal capacitance per unit area, $\Delta x \rho c$, Btu/ft^2-$^\circ$F $\left(J/m^2\text{-}^\circ C\right)$
C_S	solar radiation constant, Btu/ft^2-hr $\left(W/m^2\right)$
c	specific heat, Btu/lbm-$^\circ$F (J/kg-$^\circ$C)
$\overline{D}$	vector from spacecraft to center of earth
e	orbit eccentricity, dimensionless
F	geometric shape factor for a spinning sun-oriented planar element, dimensionless
H	distance between spacecraft and center of earth, nautical miles
h	orbit altitude, nautical miles
h_c	forced convection heat-transfer coefficient, Btu/ft^2-hr-$^\circ$F $\left(J/m^2\text{-}s\text{-}^\circ C\right)$

I	orbit inclination measured from equatorial plane, deg
i	ecliptic inclination measured from equatorial plane, deg
K	earth gravitational field constant, nautical miles^3/hr^2
k	thermal conductivity, Btu/ft-hr-^{o}F (J/m-s-^{o}C)
$L(\xi)$	length of cylindrical module at circumferential position ξ, ft (m)
l	wall thickness, ft (m)
$\overline{M}$	spacecraft angular-momentum vector
$\overline{N}(\xi)$	vector normal to spacecraft surface element at circumferential position ξ
Q	radiant heat flux absorbed by spacecraft surface area, Btu/ft^2-hr $\left(W/m^2\right)$
Q_{tot}	total radiant heat flux absorbed by spacecraft, $Q \times$ Area, Btu/hr (W)
q	radiant heat flux incident on spacecraft surface area, Btu/ft^2-hr $\left(W/m^2\right)$
q_c	passive heat transfer rate, Btu/hr (W)
R	thermal resistance, $\Delta x/k$, ft^2-hr-^{o}F/Btu $\left(m^2\text{-s-}^{o}C/J\right)$
R_E	mean radius of earth, nautical miles
r	radius, ft (m)
T	temperature, ^{o}F (^{o}C)
$\overline{T}$	temperature, ^{o}R (^{o}K)
$\dot{T}$	time derivative of temperature, ^{o}F/hr (^{o}C/s)
t	time, hr (s)
X,Y,Z	inertial coordinate frame where Z-axis coincides with north pole and X-axis is alined with vernal equinox (see fig. 2)

X',Y',Z'	rectangular coordinate frame with Z'-axis normal to orbit plane and X'-axis coinciding with earth-spacecraft line (see fig. 2)
X'',Y'',Z''	rectangular coordinate frame with Z''-axis normal to ecliptic plane and X''-axis coinciding with earth-sun line (see fig. 2)
x	wall coordinate, ft (m)
α	absorptivity to solar radiation, dimensionless
α_L	angle between line from spacecraft to center of earth and line from spacecraft to element on earth surface at terminator, deg
β	right ascension of ascending orbit node measured in equatorial plane (zero at vernal equinox), deg
γ	spacecraft position angle measured in orbit plane (zero at ascending orbit node), $\gamma_p + \eta$, deg
γ_p	argument of orbit perigee measured in orbit plane (zero at ascending orbit node), deg
Δ	finite difference operator, dimensionless
ϵ	total hemispherical emissivity, dimensionless
η	spacecraft position angle measured in orbit plane (zero at orbit perigee), deg
η_s	angle between line from center of earth to sun and line from center of earth to spacecraft, deg
ξ	angle between vector normal to spacecraft surface element and spacecraft angular momentum vector, deg
ρ	density, lbm/ft^3 (kg/m^3)
σ	Stephan-Boltzmann radiation constant, $Btu/ft^2\text{-}hr\text{-}{}^oR^4$ $(W/m^2\text{-}{}^oK^4)$
ω	angular velocity, radians/sec

Ω	position angle of sun measured in the ecliptic plane (zero at vernal equinox), deg
$\Big\vert_{x=x_0(+)}$	right-hand limit as x approaches x_0
$\Big\vert_{x=x_0(-)}$	left-hand limit as x approaches x_0

Subscripts:

Al	aluminum
air	cabin air
e	earth thermal
ent	shadow entrance
exit	shadow exit
f	foam
i	inner wall surface
j	integer
N,n	integers
p	perigee
r	earth-reflected solar
s	solar
space	space environment

ANALYSIS

Development of Heat-Flow Equations

The space station consists of six cylindrical modules arranged in the shape of a hexagon and connected by three spokes to a central hub which provides docking facilities. (See fig. 1 and ref. 3.) The normal mode of operation calls for the station to be spinning about a vector normal to the plane of the hexagon and alined toward the sun. Because of symmetry in the hexagonal station and because negligible direct and reflected radiation from one portion of the station to another is assumed (since subtended angles are generally small), one of the cylindrical modules is representative of the complete station.

A schematic drawing of the assumed basic wall structure (excluding structural members such as ring stiffeners and longerons) is shown in figure 3. As shown, the wall is essentially a five-layer composite. On the outside is a thick layer of polyurethane foam; on the inside is a thick layer of aluminum honeycomb with a polyurethane-foam-filled core. These layers are separated and covered inside and out by thin aluminum sheets.

During an equilibrium orbit, the net heat flow between the internal environment of a module and the enclosing wall surface equals the net heat flow through its wall structure. If the former heat transfer is assumed to occur solely by forced convection (this assumption is discussed later in connection with boundary conditions), the latter (passive) heat-transfer rate through the wall is given by

$$q_c = \frac{h_c r_i}{t} \int_0^t \int_0^{2\pi} L(\xi)\left[T_{air} - T_i(\xi,t)\right] d\xi \, dt \tag{1}$$

where from figure 4 the length $L(\xi)$ of the cylindrical module at circumferential position ξ is given,

$$\left.\begin{aligned} &\text{in feet, by} \quad L(\xi) = 69.2269 + 5.7731 \sin \xi \\ &\text{in meters, by} \quad L(\xi) = 21.1004 + 1.7596 \sin \xi \end{aligned}\right\} \tag{2}$$

and the inner wall surface temperature $T_i(\xi,t)$ is found by solving Fourier's heat equation subject to appropriate boundary conditions.

If negligible heat flow is assumed in the circumferential and longitudinal directions and the slight wall curvature is neglected, the Fourier heat equation reduces to

$$\frac{\partial^2 T}{\partial x^2} = \frac{\rho c}{k} \frac{\partial T}{\partial t} \tag{3}$$

In terms of the physical wall illustrated in figure 5(a), equation (3) requires that there be two paths of heat conduction through the honeycomb with no cross conduction between the two.

If a digital computer is employed in the study, both independent variables must be differenced. However, since an analog computer was to be used to solve the equations, there existed an option for allowing one of the independent variables to be continuous. In this study, the time variable was made continuous and finite differences were used for the linear dimension. This choice not only assures the numerical stability of the solution, but allows convenient handling of the boundary conditions (ref. 4) and the thermal properties of the wall which are discontinuous functions of position.

If a second-order correct central difference approximation to the spatial derivative is employed, equation (3) becomes

$$\frac{\rho c}{k}\frac{\partial T}{\partial t}\bigg|_{x_j} = \frac{\partial^2 T}{\partial x^2}\bigg|_{x_j} = \frac{\left(T_{j-1} - 2T_j + T_{j+1}\right)}{(\Delta x_j)^2} + 0\left(\Delta x_j^2\right) \tag{4}$$

If the remainders $0\left(\Delta x_j^2\right)$ are neglected, the resulting differential equations governing the heat flow per unit area through the wall in a radial direction for the nine selected node positions of figure 5(b) can be written as

$$\dot{T}_j = \frac{1}{R_n C_n}\left(T_{j-1} - 2T_j + T_{j+1}\right) \tag{5}$$

The values of thermal resistance R_n and thermal capacitance C_n are shown in table II; these values were computed from the thermal properties (assumed constant for this simplified analysis) and physical dimensions of the wall presented in table I. The increment sizes must be chosen to bound the truncated remainder to a small value. It is interesting to note that the solutions on an analog computer with t continuous appear "satisfactory even for rather large values of Δx" (ref. 5) as opposed to a digital-computer solution where the increment sizes $\left(\Delta t \text{ and } \Delta x_j\right)$ must be chosen not only to bound the two truncation errors, but in some cases to insure numerical stability.

Each layer of the wall structure is thermally coupled to its environment. This thermal coupling is expressed as a set of boundary conditions describing the mode of heat transfer at the interior-wall surface, the interfaces of the composite layers, and the exterior-wall surface. Consideration of these boundary conditions yields additional equations which can be approximated by first-order correct forward and backward differences.

Interior wall.- If all internal heat transfer (i.e., metabolic and equipment heat) to the interior wall surface is assumed to occur by convection, the boundary condition to be satisfied is

$$k_{Al}\left.\frac{\partial T}{\partial x}\right|_{x=l\,(-)} \cong \frac{k_{Al}}{\Delta x_3}\left(T_{15} - T_{14}\right) + 0(\Delta x) = -h_c\left(T_{air} - T_{15}\right) \tag{6}$$

This assumption was made because of the many uncertainties regarding the time-dependent internal distribution of onboard heat-producing components; which, even if known, would be difficult to describe. However, consideration of human comfort will undoubtedly influence the dependence on forced convection as a mode of heat transfer in manned spacecraft.

Interfaces.- If zero contact resistance is assumed at all interfaces between materials, the boundary condition to be satisfied at the jth interface is then

$$k_j\left.\frac{\partial T}{\partial x}\right|_{x=x_j(-)} = k_{j+1}\left.\frac{\partial T}{\partial x}\right|_{x=x_j(+)}$$

where the subscripts j and j+1 refer to the two dissimilar materials forming the interface. This assumption is reasonable if it is assumed that a good bond is present at these interfaces. Realistically, the joint resistances at these interfaces should be determined experimentally. Unfortunately, the mode of heat transfer through these interfaces is not well understood and prior experimental data regarding this problem have proved unreliable because of data scatter and the general inability to reproduce experimental results (ref. 6). The resulting boundary condition obtained from finite difference approximation is

$$k_j\left(\frac{T_{j-1} - T_j}{\Delta x_j}\right) = k_{j+1}\left(\frac{T_j - T_{j+1}}{\Delta x_{j+1}}\right) + 0\left(\Delta x_j, \Delta x_{j+1}\right) \tag{7}$$

Exterior wall.- When all heat transfer at the exterior wall surface is assumed to occur by radiation, the boundary condition to be satisfied is

$$-k_{Al}\left.\frac{\partial T}{\partial x}\right|_{x=0(+)} \cong -\frac{k_{Al}}{\Delta x_1}\left(T_2 - T_1\right) = Q(\xi,t) - \sigma\epsilon\left(\overline{T}_1^4 - \overline{T}_{space}^4\right) \tag{8}$$

where $\overline{T}_{space}^4$ is small and can be neglected, and $Q(\xi,t)$, the absorption rate of external radiant energy from the sun, the earth, and sunlight reflected by the earth, is discussed in appendix A.

To aid in the solution of equations (1) and (5), the cylindrical module is approximated by a 12-sided polyhedron as shown in figure 4; equation (1) can then be approximated by

$$q_c = \sum_{N=1}^{12} q_c(\xi_N) \tag{9}$$

where

$$q_c(\xi_N) = \frac{h_c r_i}{t}\left(\frac{\pi}{6}\right) L(\xi_N) \int_0^t \left[T_{air} - T_{15}(\xi_N, t)\right] dt \tag{10}$$

For the spinning case, the incident external thermal energy is symmetric about the angular-momentum vector and only six sides need be considered (i.e., $\xi_N = 15^o$, 45^o, 75^o, 105^o, 135^o, and 165^o).

Analog-Computer Equations

Equation (5) for the first aluminum sheet (j = 2, n = 1) places serious burdens on the computer used, analog or digital. The coefficient $\left(1/R_1C_1 \approx 10^6/\text{hr}\right)$ is large, and the temperature differences are small, that is, $\left[(T_1 - 2T_2 + T_3) \approx 10^{-5}\ ^oF \text{ or } ^oC\right]$. Hence, much precision is required to evaluate the derivative without loss of significance. Perturbation about some mean temperature, although helpful, will not eliminate this difficulty. Time scaling the analog computer is of no practical use because of the great dissimilarities in thermal properties and linear dimension of the various wall layers as shown in tables I and II.

A general technique to eliminate this loss of significance is described in appendix B. The technique involves judicious substitution of the boundary conditions into equation (5), after which the following simplifying assumptions can be made without introducing serious errors into the computation:

$$T_1 \cong T_2 \cong T_3$$

$$T_6 \cong T_7$$

$$T_{14} \cong T_{15}$$

If the remainders are neglected, the computer equations (eqs. (5) to (8) and eq. (10)) are

$$\dot{T}_1 = K_1\left[K_2 Q(\xi_N, t) - \sigma\epsilon \overline{T}_1^4 + K_3(T_4 - T_1)\right] \tag{11}$$

$$\dot{T}_4 = K_4(T_1 - 2T_4 + T_5) \tag{12}$$

$$\dot{T}_5 = K_4\left(T_4 - 2T_5 + T_6\right) \tag{13}$$

$$\dot{T}_6 = K_5\left[K_6T_5 - \left(2 - K_7 - K_8\right)T_6 + K_9T_9 + K_{10}T_{11}\right] \tag{14}$$

$$T_8 = K_8T_6 + K_9T_9 + K_{10}T_{11} \tag{15}$$

$$\dot{T}_9 = K_{11}\left(T_8 - 2T_9 + T_{10}\right) \tag{16}$$

$$\dot{T}_{10} = K_{11}\left(T_9 - 2T_{10} + T_{13}\right) \tag{17}$$

$$\dot{T}_{11} = K_{12}\left(T_8 - 2T_{11} + T_{12}\right) \tag{18}$$

$$\dot{T}_{12} = K_{12}\left(T_{11} - 2T_{12} + T_{13}\right) \tag{19}$$

$$T_{13} = K_8T_{15} + K_9T_{10} + K_{10}T_{12} \tag{20}$$

$$\dot{T}_{15} = K_5\left[K_9T_{10} + K_{10}T_{12} - \left(2 - K_8 - K_{13}\right)T_{15} + K_{14}T_{air}\right] \tag{21}$$

and

$$q_c\left(\xi_N\right) = K_{15}\left(\xi_N\right)\int_0^t \left[T_{air} - T_{15}\left(\xi_N, t\right)\right] dt \tag{22}$$

where the coefficients K_n are defined in terms of the equivalent network parameters by

$$K_1 = \frac{1}{R_1C_1} \qquad K_2 = R_1$$

$$K_3 = \frac{R_1}{R_1 + R_2} \qquad K_4 = \frac{1}{R_2C_2}$$

$$K_5 = \frac{1}{R_3C_3} \qquad K_6 = \frac{R_2}{R_2 + R_3}$$

$$K_7 = \frac{R_3}{R_2 + R_3} \qquad K_8 = \frac{R_4R_5}{R_4R_5 + R_3R_5 + R_3R_4}$$

$$K_9 = \frac{R_3R_5}{R_4R_5 + R_3R_5 + R_3R_4} \qquad K_{10} = \frac{R_3R_4}{R_4R_5 + R_3R_5 + R_3R_4}$$

$$K_{11} = \frac{1}{R_4C_4} \qquad K_{12} = \frac{1}{R_5C_2}$$

$$K_{13} = \frac{R_3}{R_3 + R_6} \qquad K_{14} = \frac{R_6}{R_3 + R_6}$$

and

$$K_{15}(\xi_N) = \frac{h_c r_i}{t}\left(\frac{\pi}{6}\right)L(\xi_N)$$

Equations (11) to (22) were programed on a general-purpose analog computer. The analog circuit for this system of equations is shown schematically in figure 6 where it should be noted that the coefficients of T_{11} and T_{12} in equations (15) and (20) were too small for consideration. The absorption rate of external thermal energy $Q(\xi_N,t)$ was supplied by a function generator which was programed from a digital-computer solution of equations (A1) to (A10).

To verify the analog circuitry, the governing equations were linearized by replacing the term $Q(\xi_N,t) - \sigma\epsilon\overline{T}_1^4$ by $\overline{Q}\cos\omega t$ (where $\overline{Q} = 0.2778$ Btu/ft^2-sec (3150 J/m^2-sec) and $\omega = 0.0714$ rad/sec). The linear set of equations was then solved by using the analog circuit shown in figure 6 (by disconnecting the multipliers and programing $\overline{Q}\cos\omega t$ on the function generator). These equations were also solved analytically by using the impulse response technique (one-dimensional Green's function). See reference 7.

Comparison of the two solutions is shown in figure 7. The small difference in the solutions is attributed to slight errors in that part of the analog circuit which excluded the multipliers.

RESULTS AND DISCUSSION

The system of equations (11) to (22) derived for a planar element of the composite wall was applied to each of the planar sides positioned by ξ_N for several surface optical property combinations. Figure 8 shows the resultant outer-wall surface-temperature histories for a circular 200-nautical-mile minimum sunlight orbit (orbit wherein the position of the sun is colinear with the intersection of the orbital and ecliptic planes) and a constant air temperature of 70° F (21° C). As illustrated by the figure, a wide variation in temperature is possible for each side depending on the optical coating selected.

If, at a given instant, a large circumferential temperature gradient exists, the resultant thermal stress may cause delamination of the bonded joint between wall layers. If such a delamination occurred, it would not only alter the thermal characteristics of the wall, but might affect the structural integrity of the vehicle. Thus, a coating distribution was selected to reduce the circumferential temperature gradient. This distribution is shown in table III. Figure 9(a) shows the outer-wall surface-temperature distribution for the selected set of coatings. The corresponding internal-wall surface-temperature distribution is shown in figure 9(b).

The noon orbital position (point of the closest approach of the vehicle to the sun) in figure 9 was selected as representative of an extreme circumferential temperature gradient in order to examine the temperature distribution through the wall structure of the vehicle. Figure 10 shows this result. Of interest is the small temperature differences which exist across the face of the thin aluminum sheets. In an a priori fashion this fact justifies the previous assumption of small temperature differences used in developing the equations.

For the selected coating distribution, the external and internal surface temperature histories were then calculated for a circular 300-nautical-mile orbit for both minimum and maximum sunlight (orbit wherein the position of the sun is normal to the intersection of the orbital and ecliptic planes) conditions to bracket the design range for this space station completely. These results are shown in figures 11 and 12 for a constant air temperature of 70° F (21° C).

The passive heat-transfer capability of the cylindrical module with the selected optical coating distribution is shown as a function of the heat absorbed by the module in figure 13. Of interest, is the steady-state solution (based on an average external-wall surface temperature) which is shown for comparison. The figure shows that a steady-state solution underestimates the passive heat-transfer capability of the vehicle.

Figure 14 shows the heat absorbed by the cylindrical module having the selected optical coating distribution as a function of altitude for both minimum and maximum sunlight orbits. This figure indicates that for a given altitude the vehicle absorbs less heat for a maximum sunlight orbit than for a minimum sunlight orbit for the vehicle orientation considered. The reason for this absorption difference is that the vehicle is oriented during a maximum sunlight orbit so that it receives less earth-thermal and earth-reflected solar radiation. Together, figures 13 and 14 define the passive thermal-control capability of the cylindrical module (with the selected optical coating distribution) for the altitude range of interest.

It should be noted that equations (11) to (22) are in a form to be integrated by using standard subroutines on a digital computer. However, past experience has shown that such practice is expensive because of the long computation time which is due to the use of extremely accurate integration subroutines with too stringent error criteria. If a digital solution is considered, then a simpler approximation to the time derivative is suggested by reference 4.

CONCLUDING REMARKS

The passive thermal behavior of an example space station was determined for a range of orbit conditions from analog-computer solutions of Fourier's heat equation as

applied to the composite multilayer wall structure of the spacecraft. Comparison of steady-state and transient solutions showed that the steady-state solution underestimated the passive heat-transfer capability of the spacecraft.

Explicit use was made of Fourier's heat equation which reduced the chance of an erroneous solution that may result from intuitive approximations. Approximations such as lumping the aluminum with the foam, neglecting the thermal conductivity of the aluminum, and even neglecting completely the aluminum sheets, are not necessary and give no indication of the amount of error introduced. In this report, the errors other than truncation errors, which are predictable, are known to be compatible with the resolution of the general-purpose analog computer.

The governing heat-transfer equation can be programed directly if the composite wall layers are similar in both linear dimension and thermal properties. When great dissimilarities exist, loss of significance will occur. This loss of significance can be relieved by the technique outlined in an appendix.

The analog computer, with its usual ease of changing parameters and rapidity of solution, proved to be relatively economical. An analytical solution of linearized equations was in good agreement with the corresponding analog solution.

Results of this study are of value in the thermal design of any orbiting spacecraft since they illustrate a relatively simple procedure for determining the passive heat-transfer capability of a vehicle. Knowledge of the thermal mission requirements of the vehicle will then permit estimates of the supplemental active thermal control necessary to maintain desired temperatures. On this basis, the vehicle can either be redesigned if it appears necessary, or the present design can be analyzed more rigorously to define its thermal control requirements more precisely.

Langley Research Center,
National Aeronautics and Space Administration,
Langley Station, Hampton, Va., June 17, 1966.

APPENDIX A

DETERMINATION OF EXTERNAL THERMAL ENERGY

The external thermal energy which is absorbed by a spacecraft surface element is given as a function of element position ξ and orbit position η by

$$Q(\xi,\eta) = \left[q_s(\xi,\eta) + q_r(\xi,\eta)\right]\alpha + q_e(\xi,\eta)\epsilon \tag{A1}$$

where

$$\left.\begin{aligned} q_s(\xi,\eta) &= C_s \cos \xi \qquad \left(|\xi| < 90^o\right);\ \left(\eta_{exit} < \eta < \eta_{ent}\right) \\ q_s(\xi,\eta) &= 0 \qquad\qquad \left(|\xi| \geq 90^o\right);\ \left(\eta_{ent} \leq \eta \leq \eta_{exit}\right) \end{aligned}\right\} \tag{A2}$$

$$\left.\begin{aligned} q_r(\xi,\eta) &\cong C_s a F(\xi,\eta)\cos \eta_s \qquad \left(|\eta_s| < 90^o\right) \\ q_r(\xi,\eta) &\cong 0 \qquad\qquad\qquad\qquad \left(|\eta_s| \geq 90^o\right) \end{aligned}\right\} \tag{A3}$$

and

$$q_e(\xi,\eta) = \frac{C_s(1 - a)F(\xi,\eta)}{4} \tag{A4}$$

Time-Position Relation

The absorbed external energy $Q(\xi,\eta)$ as defined by equation (A1) can be expressed as a function of time in orbit (measured from orbit perigee) to reach orbit position η (i.e., $Q(\xi,t)$). This relation is given from reference 8 for an elliptical orbit by

$$t = \sqrt{\frac{A^3}{K}}\left[\sin^{-1}\left(\frac{e + \cos \eta}{1 + e \cos \eta}\right) - \frac{\pi}{2} - \frac{e\sqrt{1 - e^2}\sin \eta}{1 + e \cos \eta}\right] \tag{A5}$$

Geometric Shape Factor

From reference 9, the geometric shape factor $F(\xi,\eta)$ for a spinning sun-oriented planar element in equations (A3) and (A4) is given by

APPENDIX A

$$F(\xi,\eta) = B_0 + B_1(C) + B_2\left(C^2 + \frac{D^2}{2}\right) + B_3\left(C^4 + 3C^2D^2 + \frac{3}{8}D^4\right)$$

$$+ B_4\left(C^6 + \frac{15}{2}C^4D^2 + \frac{45}{8}C^2D^4 + \frac{5}{16}D^6\right) \tag{A6}$$

where

$$C = -\cos\,\xi\,\cos\,\eta_S$$

$$D = \sin\,\xi\,\sin\,\eta_S$$

and where

$$\left.\begin{aligned}
B_0 &= \frac{2}{7\pi}\left(\frac{577}{105} - 7\cos\,\alpha_L + \frac{4}{3}\cos^3\alpha_L - \frac{2}{5}\cos^5\alpha_L + \frac{4}{7}\cos^7\alpha_L\right)\\
B_1 &= \frac{1}{2}\sin^2\alpha_L\\
B_2 &= \frac{8}{7\pi}\left(\cos\,\alpha_L - 2\cos^3\alpha_L + 4\cos^5\alpha_L - 3\cos^7\alpha_L\right)\\
B_3 &= \frac{4}{7\pi}\left(-\cos\,\alpha_L + \frac{40}{3}\cos^3\alpha_L - \frac{91}{3}\cos^5\alpha_L + 18\cos^7\alpha_L\right)\\
B_4 &= \frac{8}{35\pi}\left(5\cos\,\alpha_L - 35\cos^3\alpha_L + 63\cos^5\alpha_L - 33\cos^7\alpha_L\right)\\
\alpha_L &= \sin^{-1}\left(\frac{R_E}{H}\right)\\
H &= \frac{(h_p + R_E)(1 + e)}{1 + e\,\cos\,\pi}\\
h &= H - R_E
\end{aligned}\right\} \tag{A7}$$

Attitude-Position Relation

The attitude angle $180^o - \eta_S$ shown in figure 2 defined in terms of orbit parameters for a sun-oriented vehicle can be found since (see ref. 9 for derivation)

APPENDIX A

$$\cos \eta_S = \cos \Omega(\cos \gamma \cos \beta - \sin \gamma \cos I \sin \beta)$$

$$+ (\cos i \sin \Omega)(\cos \gamma \sin \beta + \sin \gamma \cos I \cos \beta)$$

$$+ \sin i \sin \Omega \sin \gamma \sin I \tag{A8}$$

where it should be noted that $\gamma = \gamma_p + \eta$.

Shadow Entrance and Exit

Shadow entrance and exit occur when (from ref. 10):

$$\cos \eta_S = -\cos \alpha_L \tag{A9}$$

where

$$\cos \alpha_L = \sqrt{1 - \left(\frac{R_E}{H}\right)^2} \tag{A10}$$

The limits on the position of the spacecraft for receiving both solar radiation (eqs. (A2)) and earth-reflected solar radiation (eqs. (A3)) are then determined from equations (A8), (A9), and (A10).

APPENDIX B

TECHNIQUE FOR INCREASING RESOLUTION IN COMPUTATIONS

Differential equation (5) for $n = 1, 3$ and $j = 2, 5, 14$ govern the heat flow in the thin, highly conductive aluminum layers of the wall structure. Significance can be increased by judicious substitution of the algebraic boundary conditions (eqs. (6), (7), and (8)). To illustrate this, consider the following forms of equations (5), (7), and (8):

$$\dot{T}_2 = \frac{k_{Al}}{\rho_{Al} c_{Al} (\Delta x_1)^2}(T_1 - 2T_2 + T_3) \tag{B1}$$

$$\frac{k_{Al}}{\Delta x_1}(T_3 - T_2) = \frac{k_f}{\Delta x_2}(T_4 - T_3) \tag{B2}$$

$$\frac{k_{Al}}{\Delta x_1}(T_1 - T_2) = Q(\xi,t) - \sigma\epsilon \overline{T}_1^4 \tag{B3}$$

where T_1 and T_3 are the temperatures on the boundary and T_2 and T_4 are the temperatures inside the materials and are described by time derivatives. The conditions of dissimilarity in thermal properties and physical dimensions are

$$k_{Al} \gg k_f \qquad \Delta x_1 \ll \Delta x_2$$

$$\frac{k_{Al}}{\rho_{Al} c_{Al} (\Delta x_1)^2} \gg 1 \qquad \frac{k_{Al}}{\Delta x_1} \gg 1$$

Let $b_1 = \frac{k_{Al}}{\Delta x_1}$, $b_2 = \frac{k_f}{\Delta x_2}$, and $a_1 = \frac{k_{Al}}{(\Delta x_1)^2 \rho_{Al} c_{Al}}$ so that $b_1 \gg b_2$, $a_1 \gg 1$, and $b_1 \gg 1$.

It follows that

$$\frac{1}{b_1} \ll 1 \qquad \frac{b_2}{b_1} \ll 1 \tag{B4}$$

Solving equations (B2) and (B3) for T_2 and T_1, respectively, and substituting into equation (B1) gives

APPENDIX B

$$\dot{T}_2 = \frac{a_1}{b_1}\left[Q(\xi,t) - \sigma\epsilon\overline{T}_1^4 + b_2\left(T_4 - T_3\right)\right] \tag{B5}$$

where the coefficients for this equation are $\frac{a_1}{b_1}$ and $\frac{a_1 b_2}{b_1}$. From the inequalities (eq. (B4)), it follows that $\frac{a_1}{b_1} \ll a_1$ and $\frac{a_1 b_2}{b_1} \ll a_1$. The coefficients in the new form of equation (3), equation (B5), have thus been greatly reduced and the differences in the bracket are larger.

REFERENCES

1. Turner, Richard E.: Solutions and Methods of Solutions for Problems Encountered in the Thermal Design of Spacecraft. M.S. Thesis, Virginia Polytechnic Institute, 1964.

2. Mechtly, E. A.: The International System of Units - Physical Constants and Conversion Factors. NASA SP-7012, 1964.

3. Langley Research Center Staff: A Report on the Research and Technological Problems of Manned Rotating Spacecraft. NASA TN D-1504, 1962.

4. Crank, J.; and Nicolson, P.: A Practical Method for Numerical Evaluation of Solutions of Partial Differential Equations of the Heat-Conduction Type. Proc. Cambridge Phil. Soc., vol. 43, 1947, pp. 50-67.

5. Gay, B.: Comparison of Methods for Solution of the Heat Conduction Equation With a Radiation Boundary Condition. Intern. J. Heat Mass Transfer (Shorter Commun.), vol. 8, no. 3, Mar. 1965, pp. 507-508.

6. Clausing, A. M.: An Experimental and Theoretical Investigation of the Thermal Contact Resistance. ME-TN-242-3 (Grant NsG 242-62), Eng. Expt. Sta., Univ. of Illinois, July 1966.

7. Mathews, Jon; and Walker, R. L.: Mathematical Methods of Physics. W. A. Benjamin, Inc., 1964, pp. 255-263.

8. Ehricke, Krafft A.: Environmental and Celestial Mechanics. Vol. I of Space Flight, Grayson Merrill, ed., D. Van Nostrand Co., Inc., 1960.

9. Clark, Lenwood G.; and Anderson, E. Clay: Geometric Shape Factors for Planetary-Thermal and Planetary-Reflected Radiation Incident Upon Spinning and Nonspinning Spacecraft. NASA TN D-2835, 1965.

10. Hastings, Earl C., Jr.; Turner, Richard E.; and Speegle, Katherine C.: Thermal Design of Explorer XIII Micrometeoroid Satellite. NASA TN D-1001, 1962.

TABLE I.- MATERIAL PROPERTIES

Material	ρ		k		c	
	$\frac{lbm}{ft^3}$	$\frac{kg}{m^3}$	$\frac{Btu}{hr\text{-}ft\text{-}^oF}$	$\frac{J}{m\text{-}s\text{-}^oC}$	$\frac{Btu}{lbm\text{-}^oF}$	$\frac{J}{kg\text{-}^oC}$
Aluminum	173	2770	110	190	0.211	833
Polyurethane foam	1.50	24.0	.009	.016	.250	1050
Aluminum honeycomb	4.50	72.1	------	------	----	----

TABLE II.- HEAT-TRANSFER CHARACTERISTICS AND PHYSICAL DIMENSIONS

n	Δx_n		R_n		C_n	
	ft	m	$\frac{ft^2\text{-}hr\text{-}^oF}{Btu}$	$\frac{m^2\text{-}s\text{-}^oC}{J}$	$\frac{Btu}{ft^2\text{-}^oF}$	$\frac{J}{m^2\text{-}^oC}$
1	8.33×10^{-4}	2.54×10^{-4}	7.57×10^{-6}	1.34×10^{-6}	3.04×10^{-2}	5.86×10^{3}
2	2.64×10^{-2}	8.05×10^{-3}	2.93	5.03×10^{-1}	9.90×10^{-3}	2.02×10^{3}
3	1.58×10^{-3}	4.82×10^{-4}	1.44×10^{-5}	2.54×10^{-6}	5.77×10^{-2}	1.11×10^{4}
4			9.23×10^{-3}	1.63×10^{-3}	9.58×10^{-1}	1.86×10^{5}
5			3.01	5.16×10^{-1}		
6			1.00	1.76×10^{-1}		

TABLE III.- SELECTED THERMAL COATING DISTRIBUTION

ξ_N	15^o	45^o	75^o	105^o	135^o	165^o
α	0.3	0.3	0.5	0.5	0.3	0.3
ϵ	.9	.9	.5	.1	.1	.1

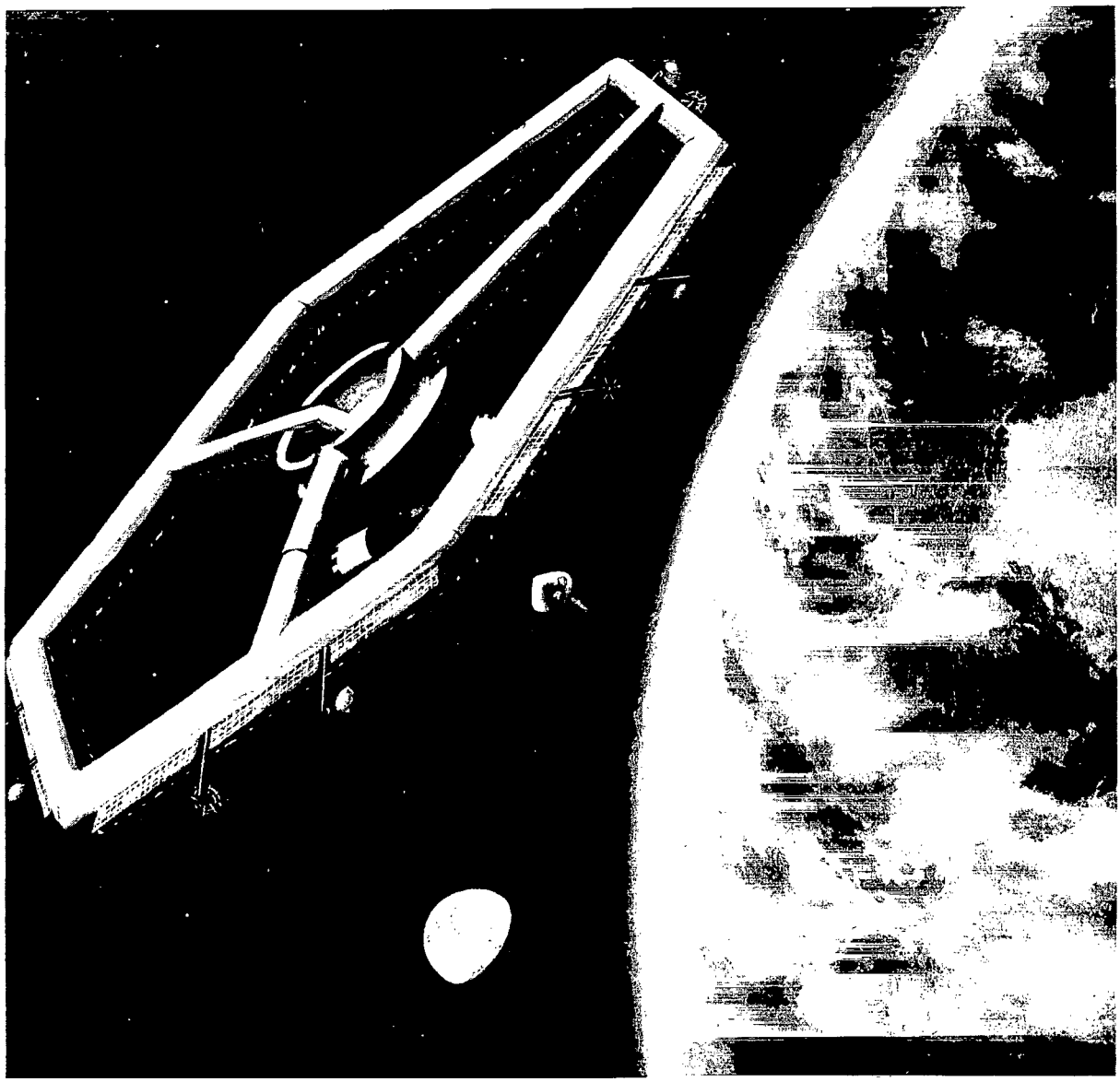

Figure 1.- Artist's concept of a 150-foot-diameter (45.7-m) hexagonal space station. L-62-8400

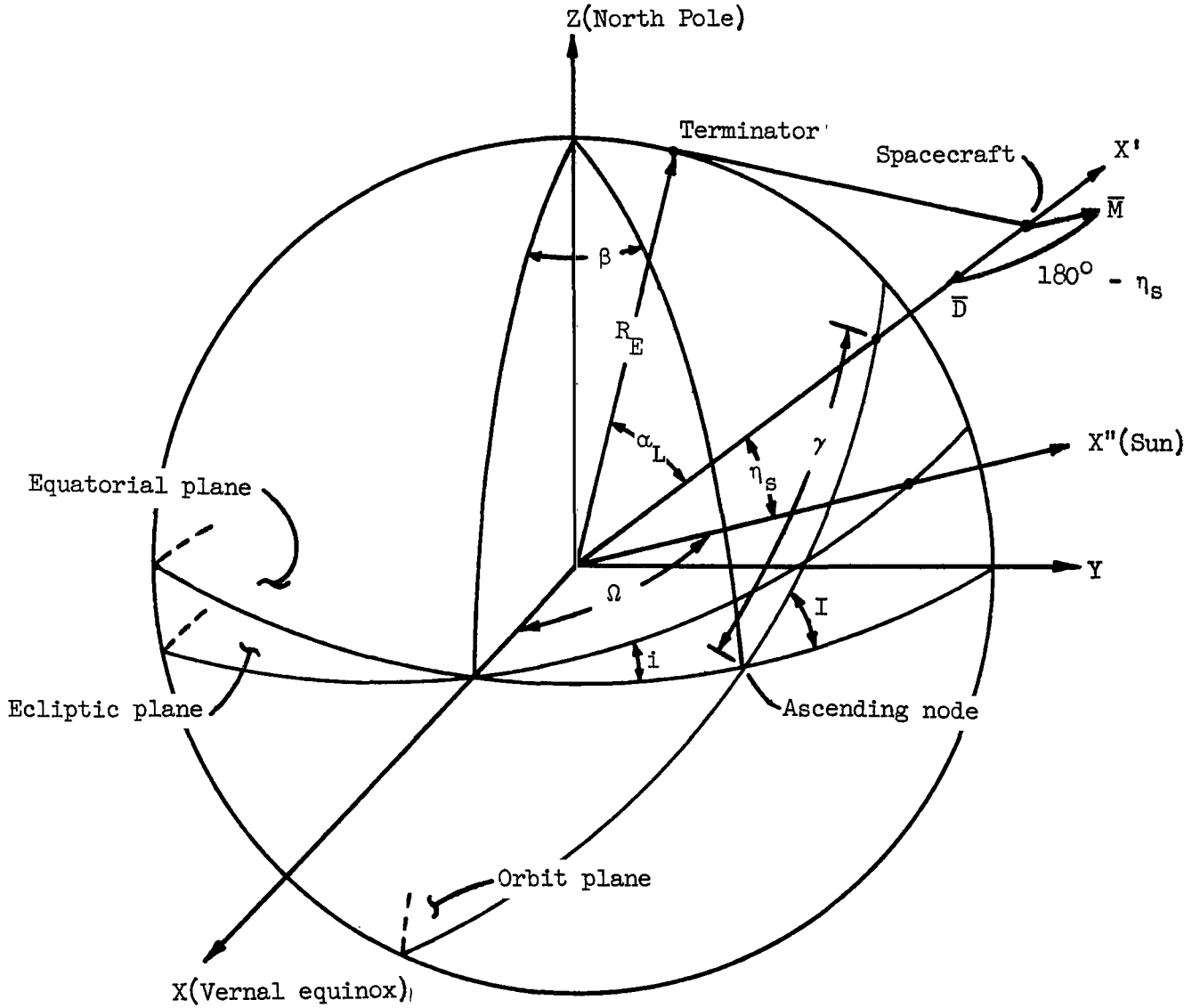

Figure 2.- Orbit geometry for a sun-oriented spacecraft.

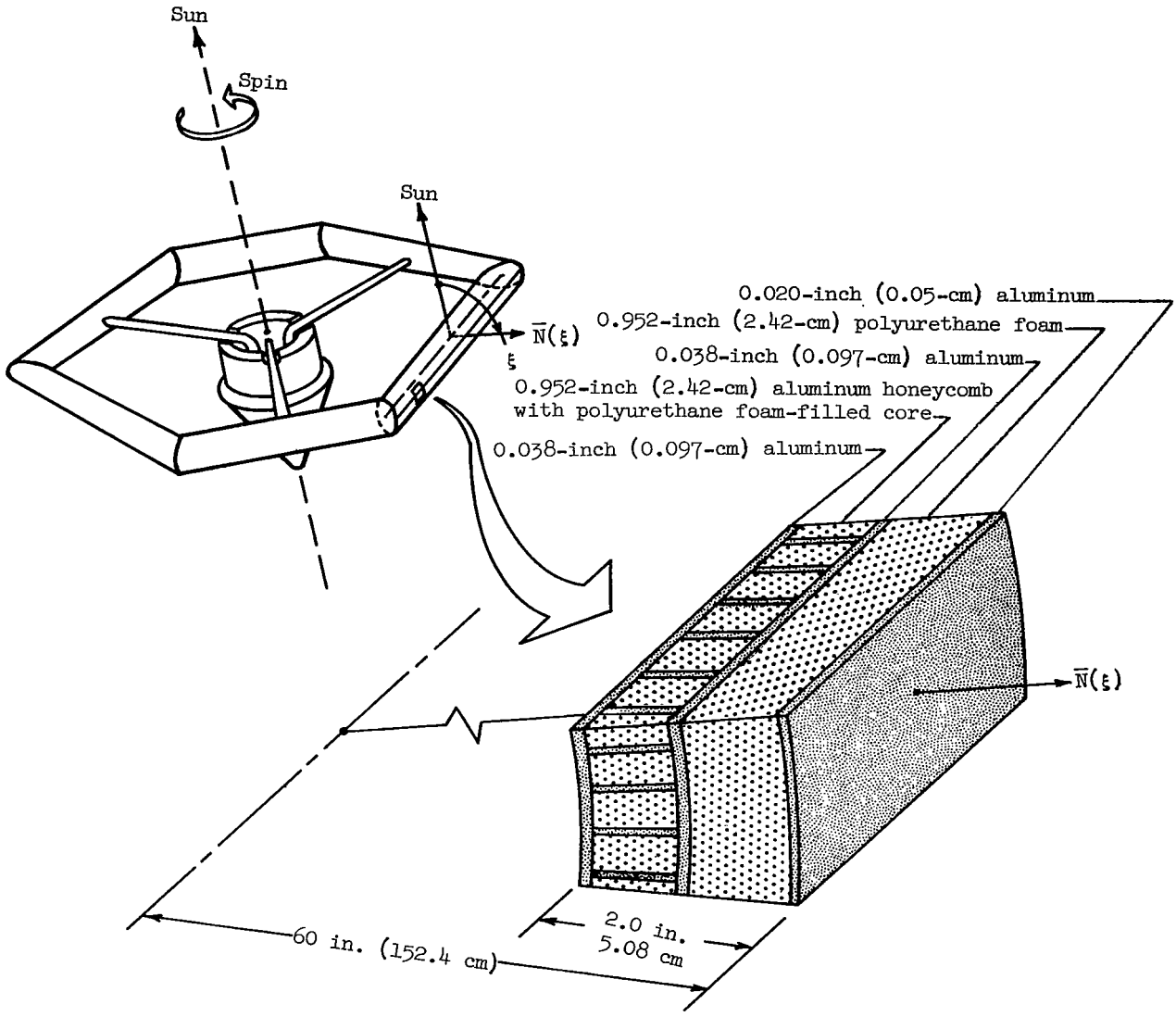

Figure 3.- Exploded sketch showing composite wall segment.

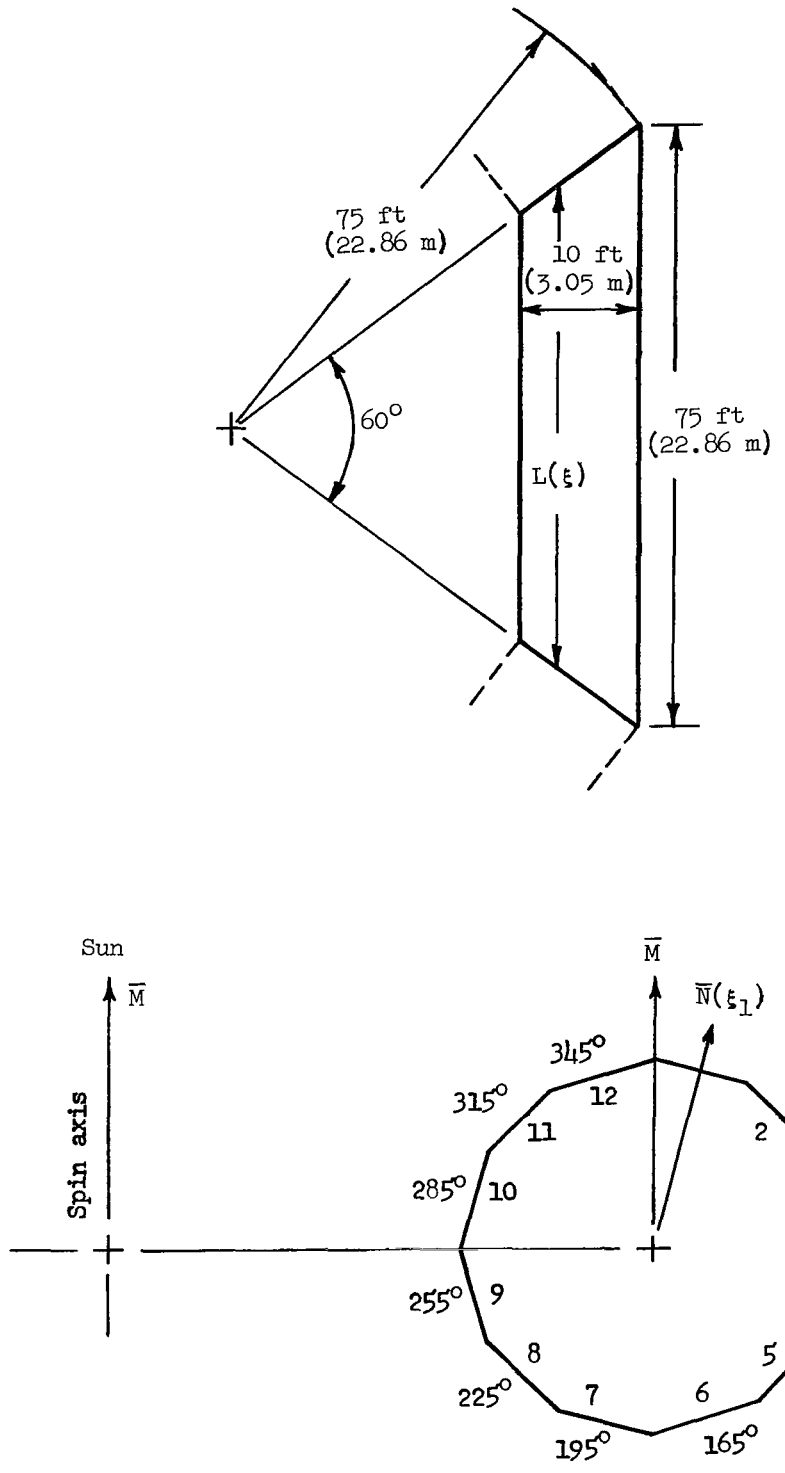

Figure 4.- Sketch showing cylindrical module dimensions and polyhedron approximation of its circular cross section.

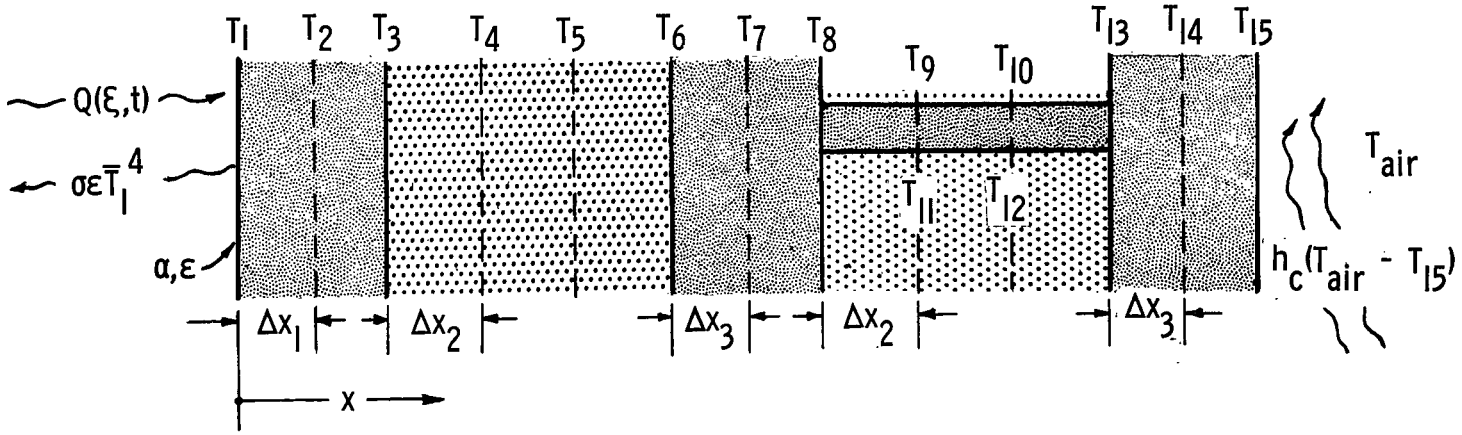

(a) Physical system showing temperature node locations.

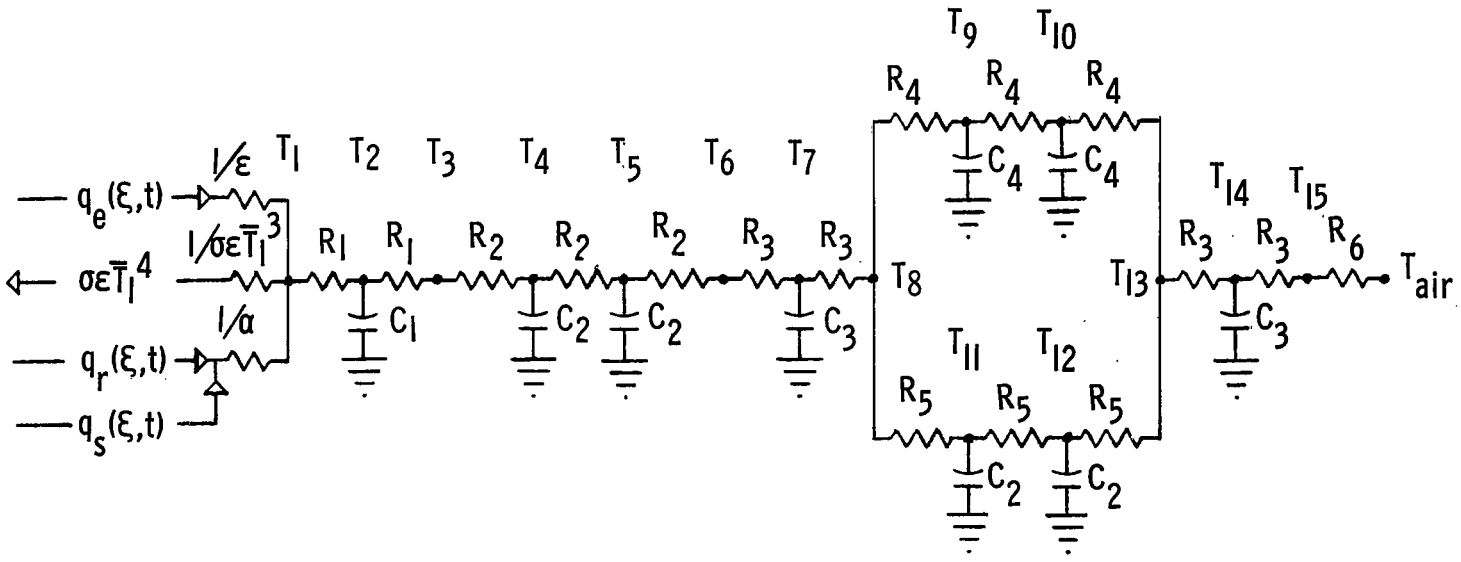

(b) Basic electrothermal circuit.

Figure 5.- Schematic of composite thermal wall.

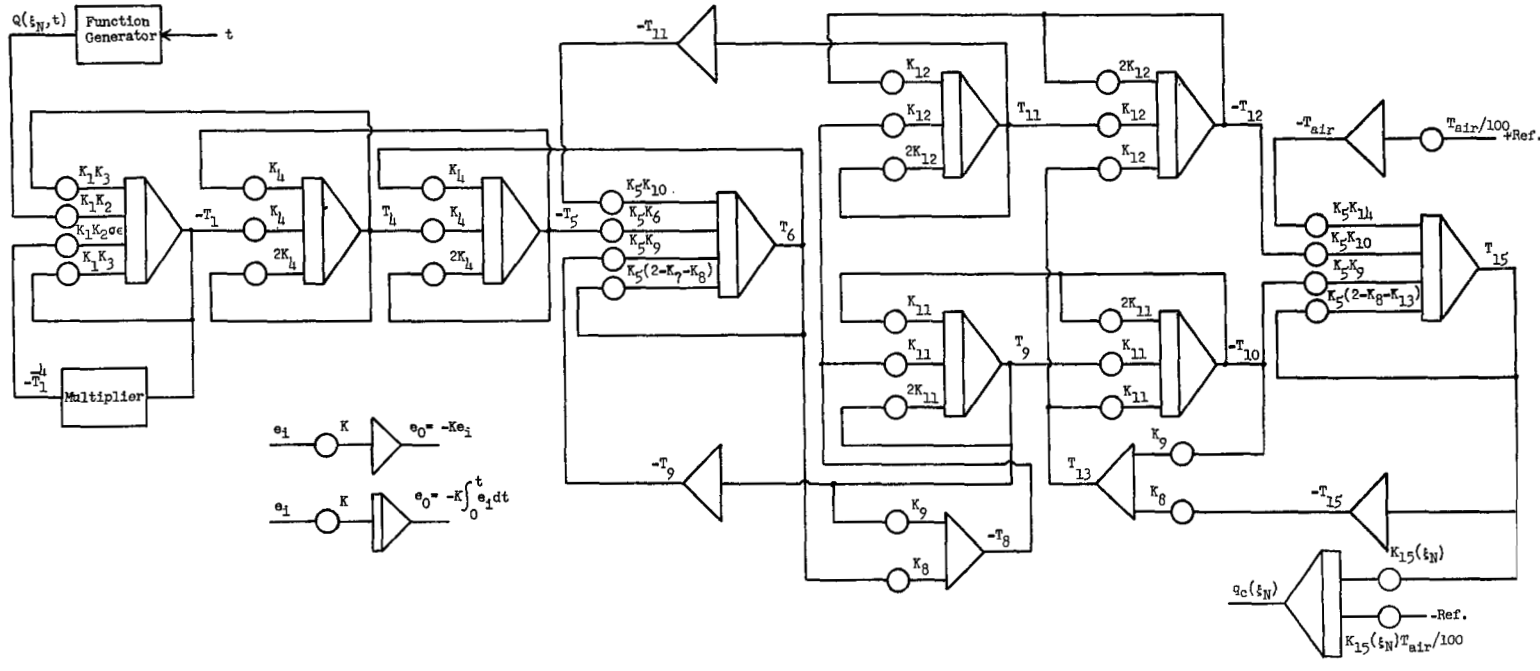

Figure 6.- Schematic of analog-computer circuit for determining the thermal behavior of a wall element of the cylindrical module.

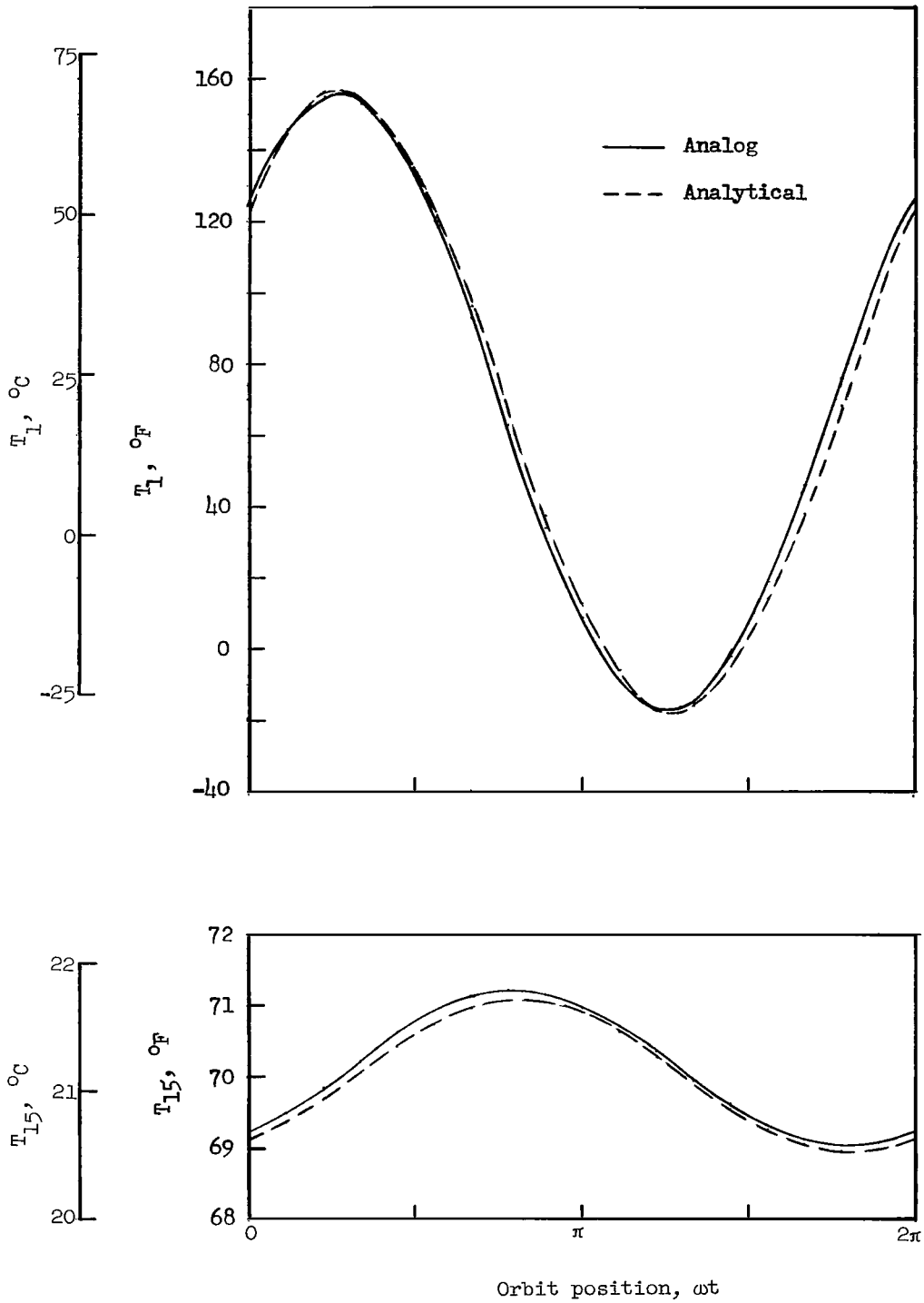

Figure 7.- Comparison of solutions of linearized equations.

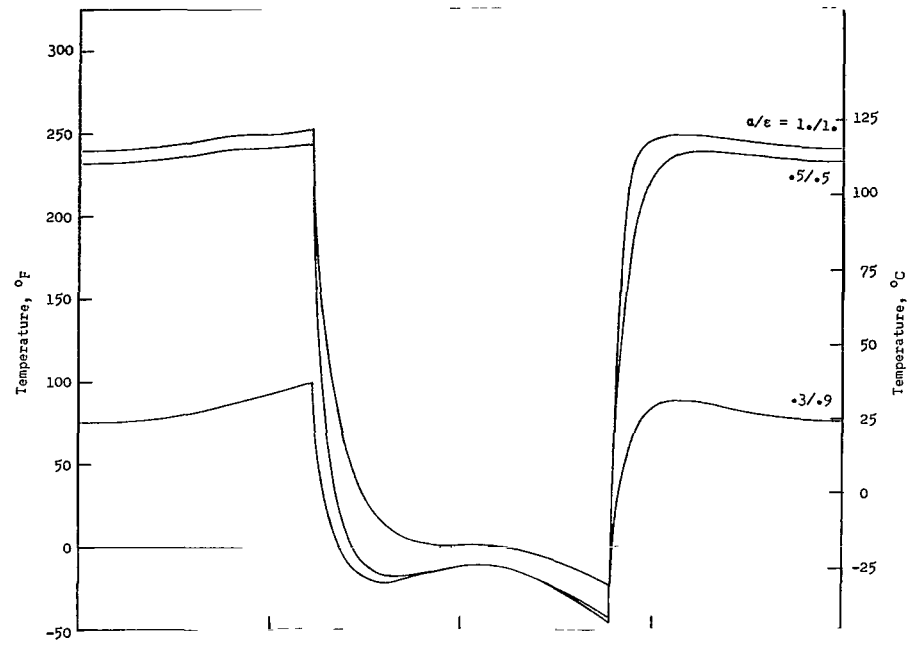

(a) $\xi = 15^0$.

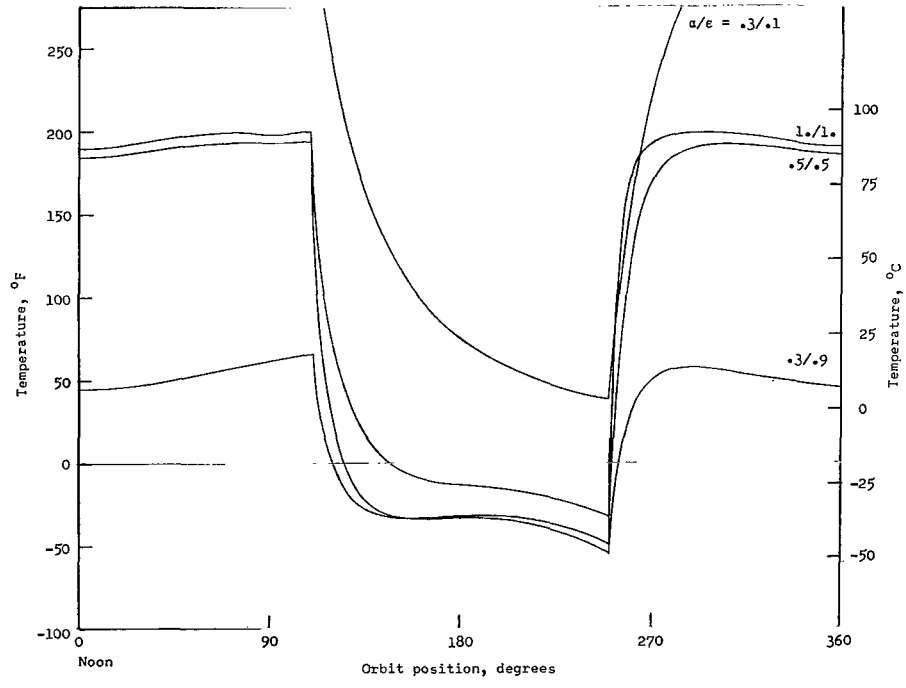

(b) $\xi = 45^0$.

Figure 8.- Variation of outer-wall surface-temperature history as a function of thermal coatings. h = 200 n.mi., $I = 28^0$, minimum sunlight, $T_{air} = 70^0$ F (21^0 C), h_c = 1.0/Btu hr-ft^2-^{0}F (0.176 J/m^2-s-^{0}C).

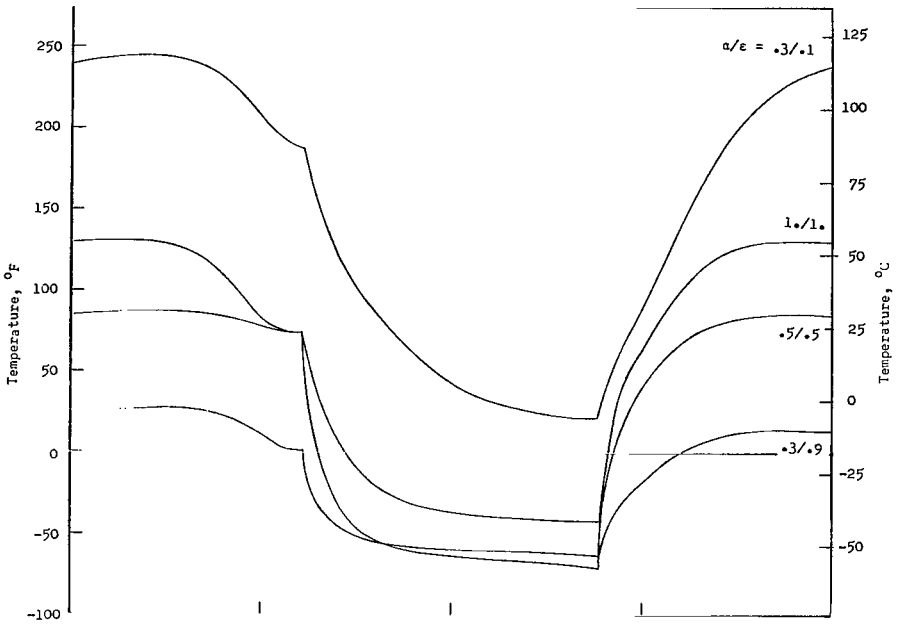

(c) $\xi = 75^0$.

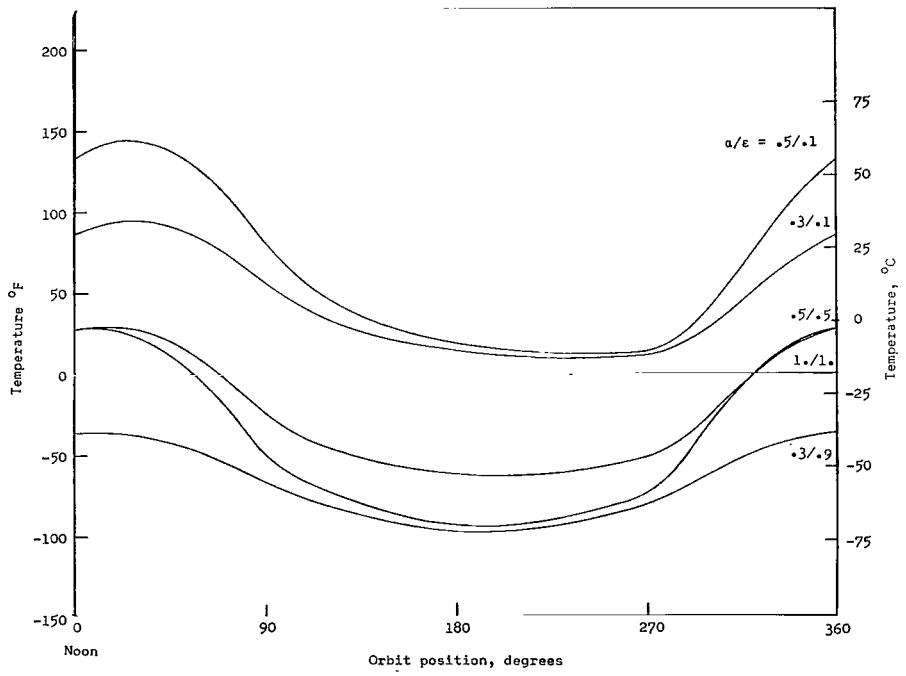

(d) $\xi = 105^0$.

Figure 8.- Continued.

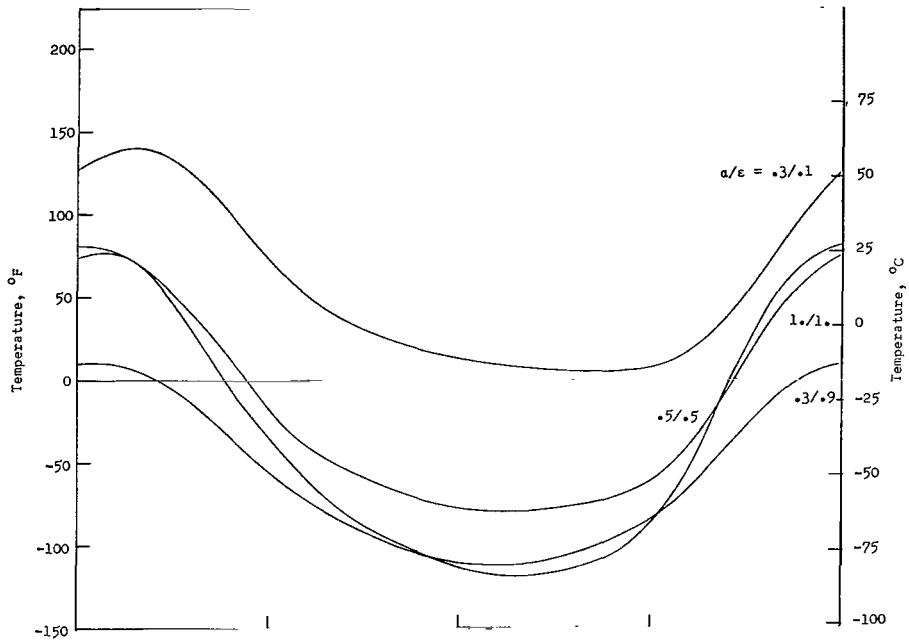

(e) $\xi = 135^{0}$.

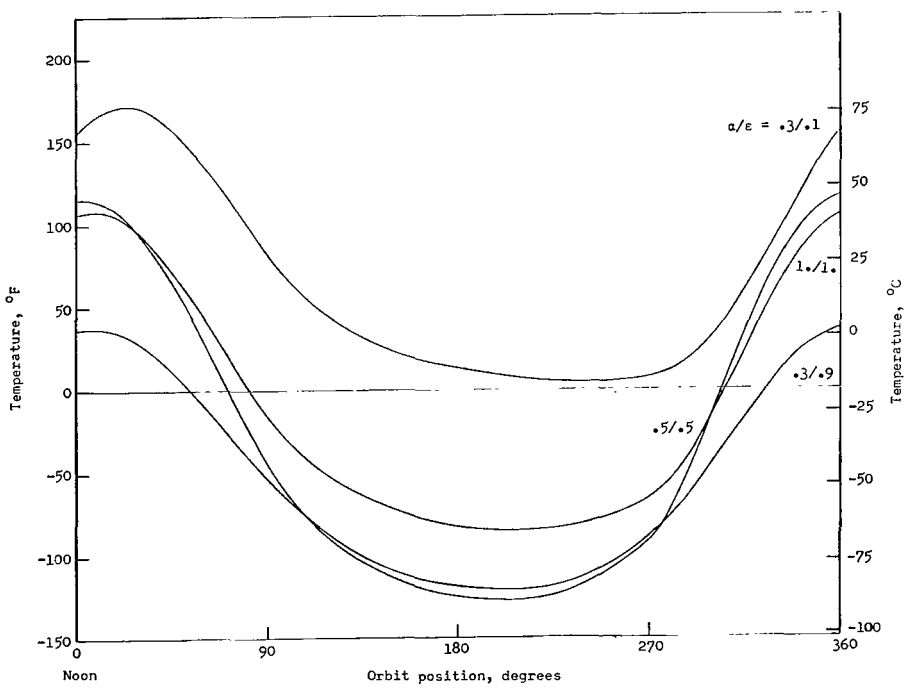

(f) $\xi = 165^{0}$.

Figure 8.- Concluded.

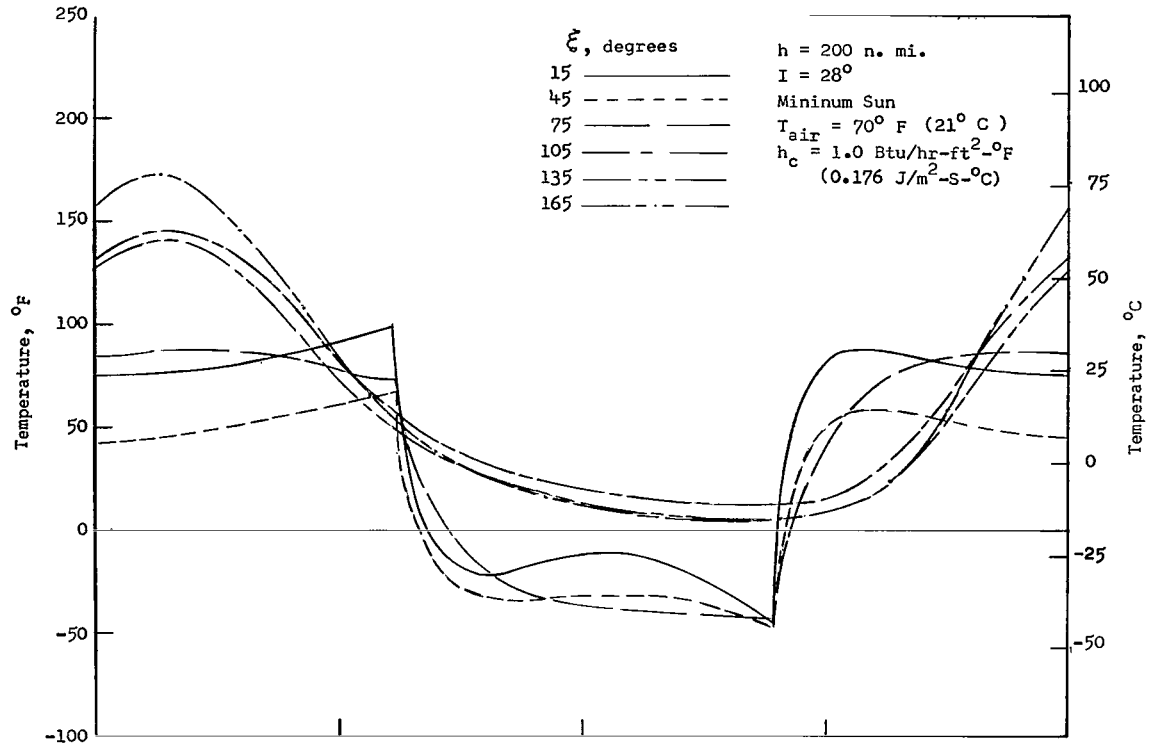

(a) Outer wall.

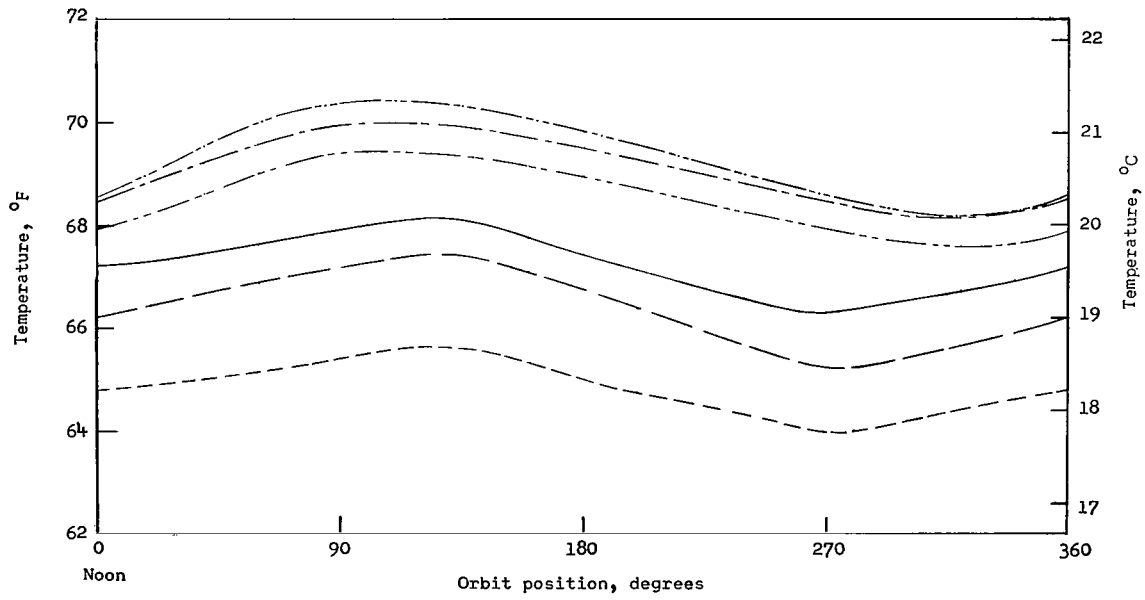

(b) Inner wall.

Figure 9.- Temperature history and temperature distribution as a function of orbit position for selected thermal coatings. (See table III.)

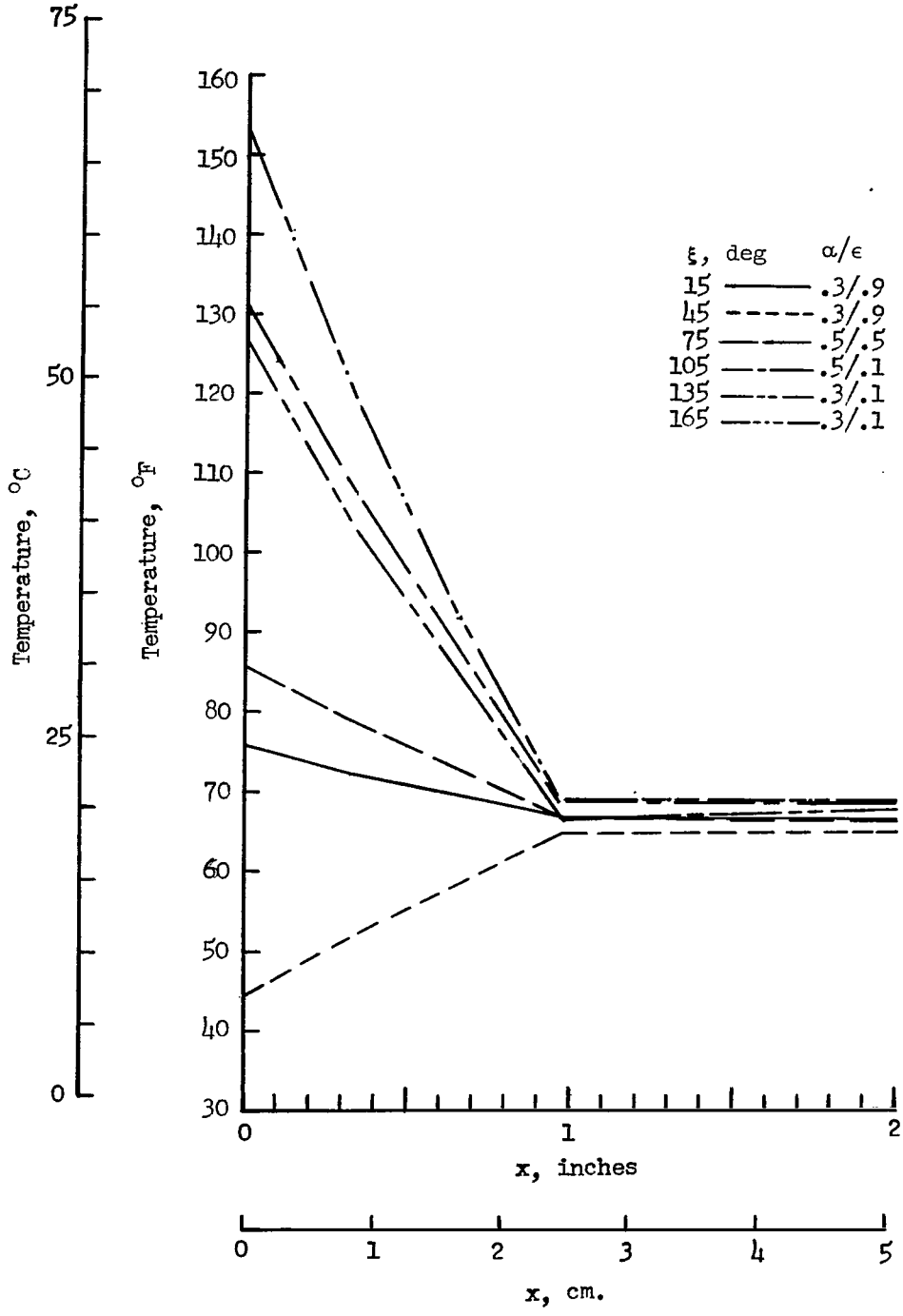

Figure 10.- Structural temperature distribution for noon orbital position. h = 200 n.mi., I = 28°, minimum sunlight, T_{air} = 70° F (21° C), h_c = 1.0 Btu/hr-ft^2-°F (0.176 J/m^2-s-°C).

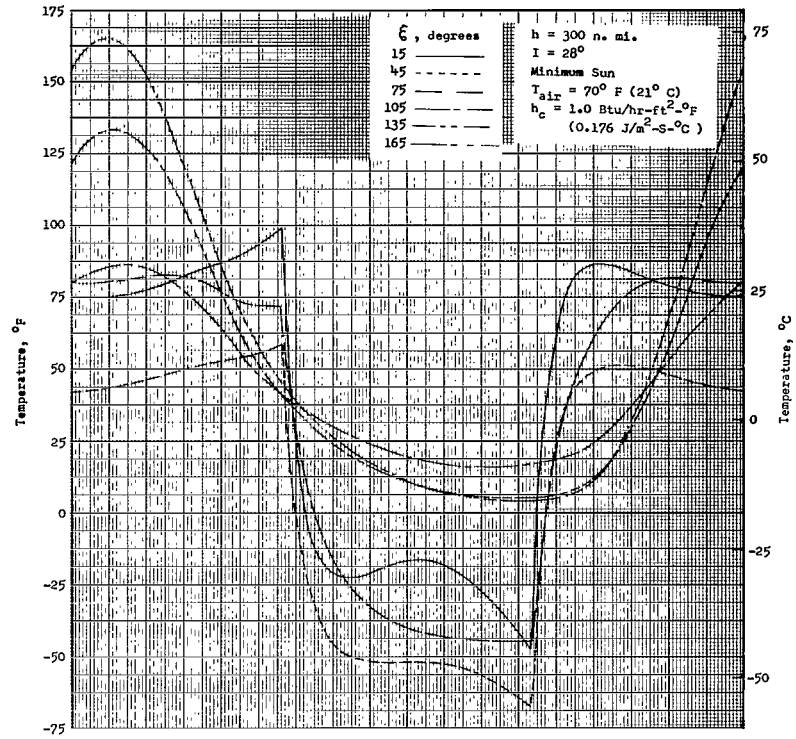

(a) Outer wall.

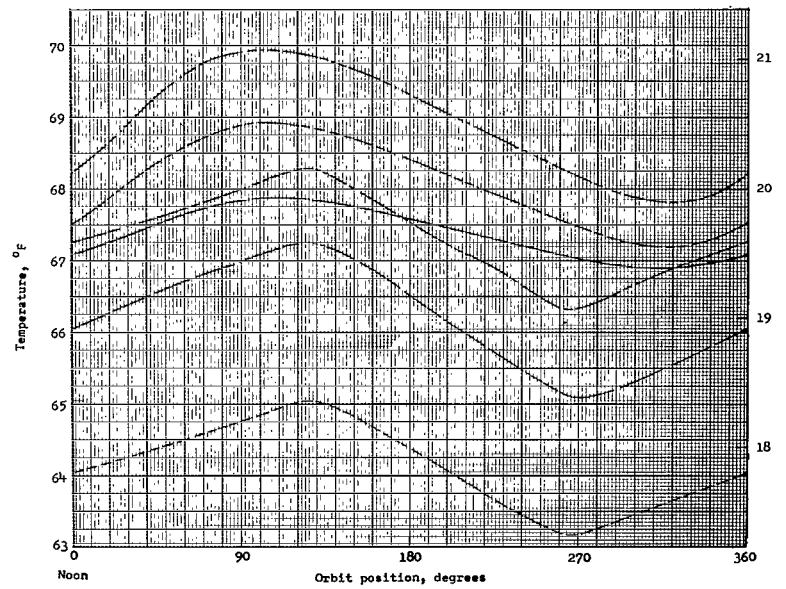

(b) Inner wall.

Figure 11.- Temperature history and temperature distribution for minimum sun as a function of orbit position for selected thermal coatings. (See table III.)

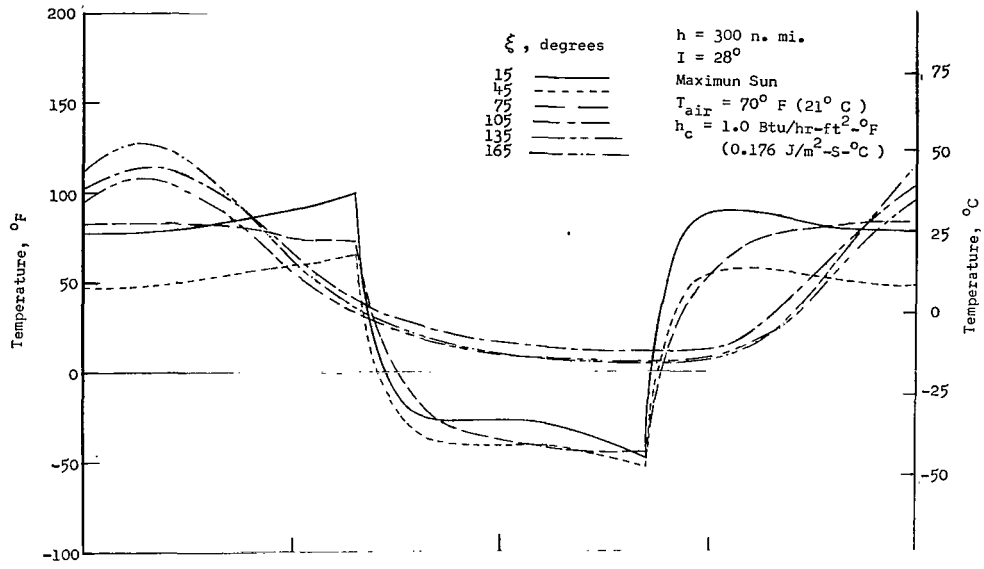

(a) Outer wall.

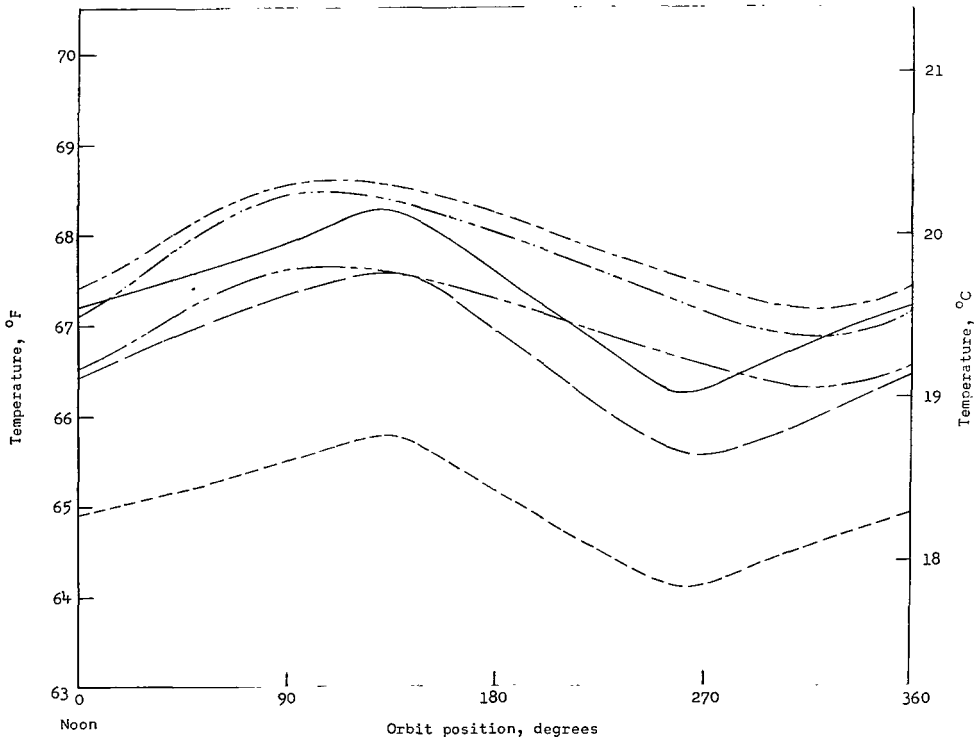

(b) Inner wall.

Figure 12.- Temperature history and temperature distribution for maximum sun as a function of orbit position for selected thermal coatings. (See table III.)

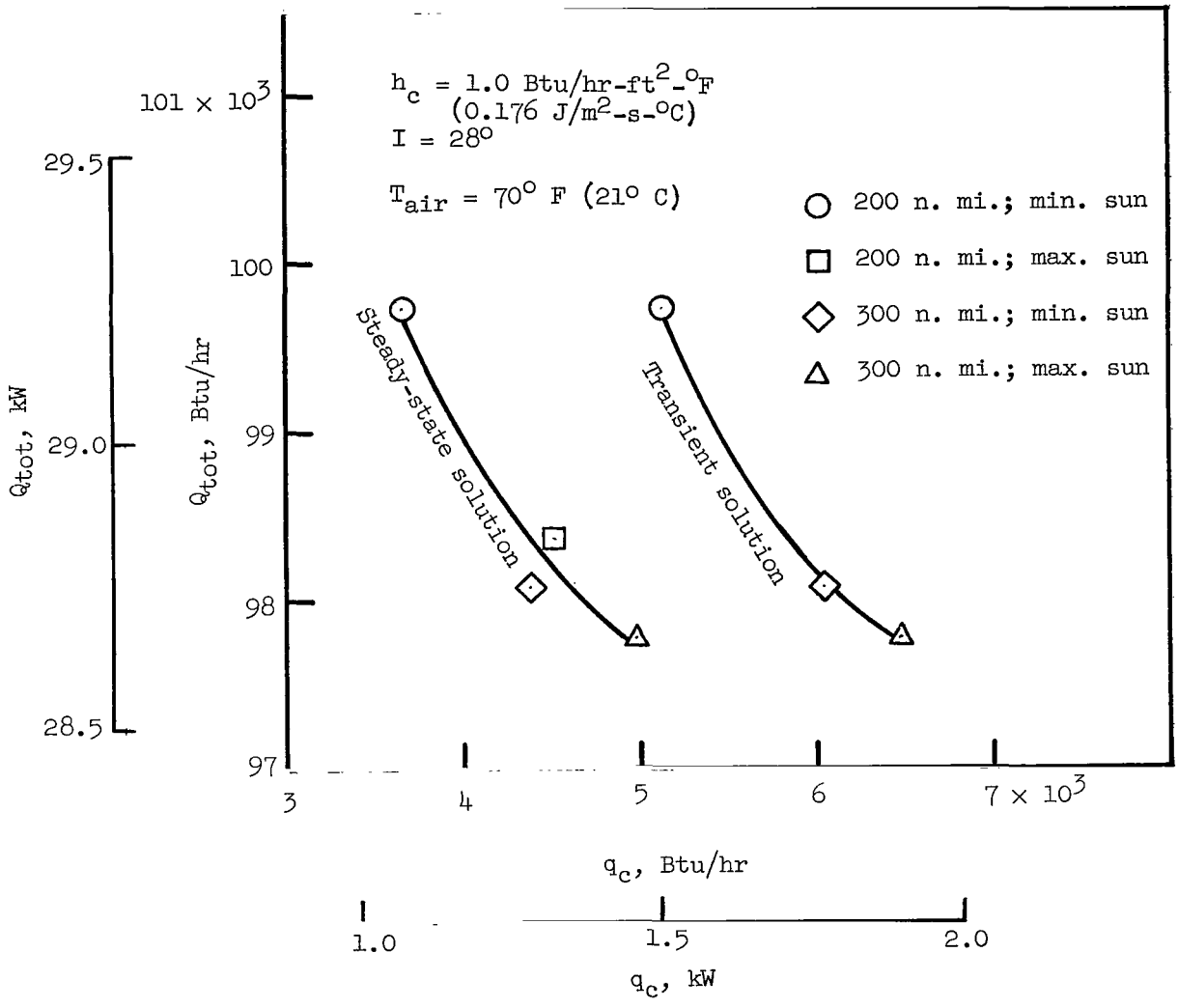

Figure 13.- Passive heat transfer as a function of heat absorbed for cylindrical module with selected coating distribution. (See table III.)

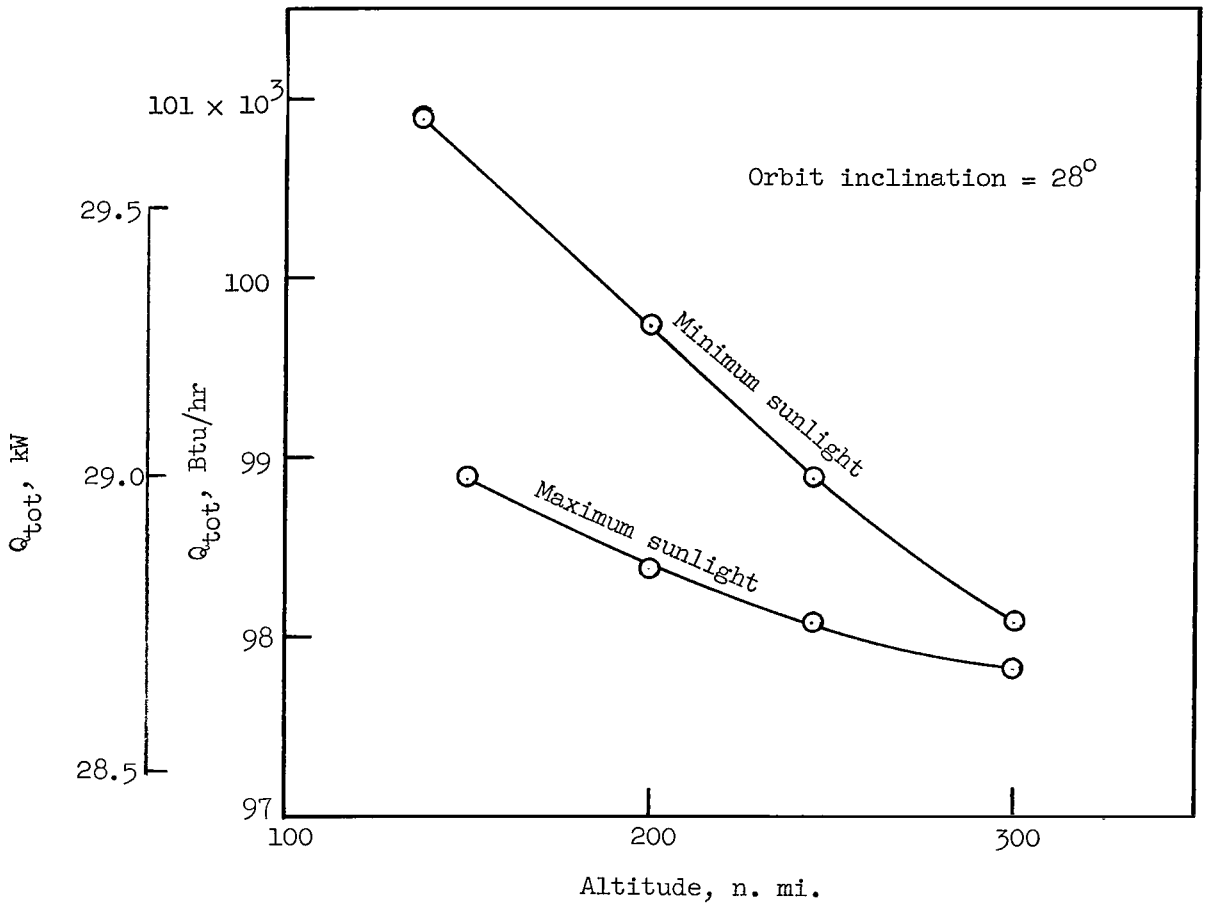

Figure 14.- Variation of heat absorbed by spinning sun-oriented cylindrical module with selected thermal coating distribution (table III) as a function of altitude.

"The aeronautical and space activities of the United States shall be conducted so as to contribute . . . to the expansion of human knowledge of phenomena in the atmosphere and space. The Administration shall provide for the widest practicable and appropriate dissemination of information concerning its activities and the results thereof."

—NATIONAL AERONAUTICS AND SPACE ACT OF 1958

NASA SCIENTIFIC AND TECHNICAL PUBLICATIONS

TECHNICAL REPORTS: Scientific and technical information considered important, complete, and a lasting contribution to existing knowledge.

TECHNICAL NOTES: Information less broad in scope but nevertheless of importance as a contribution to existing knowledge.

TECHNICAL MEMORANDUMS: Information receiving limited distribution because of preliminary data, security classification, or other reasons.

CONTRACTOR REPORTS: Technical information generated in connection with a NASA contract or grant and released under NASA auspices.

TECHNICAL TRANSLATIONS: Information published in a foreign language considered to merit NASA distribution in English.

TECHNICAL REPRINTS: Information derived from NASA activities and initially published in the form of journal articles.

SPECIAL PUBLICATIONS: Information derived from or of value to NASA activities but not necessarily reporting the results of individual NASA-programmed scientific efforts. Publications include conference proceedings, monographs, data compilations, handbooks, sourcebooks, and special bibliographies.

Details on the availability of these publications may be obtained from:

SCIENTIFIC AND TECHNICAL INFORMATION DIVISION

NATIONAL AERONAUTICS AND SPACE ADMINISTRATION

Washington, D.C. 20546